SUPPLEMENTARY INFORMATION FOR:

Imidazolylidene Cu(II) complexes: synthesis using imidazolium carboxylate precursors and structure rearrangement pathways

Nathalie Ségaud,[a] Jonathan McMaster,[b] Gerard van Koten,[c] Martin Albrecht*,[a]

a) Department of Chemistry & Biochemistry, University of Bern, Freiestrasse 3, 3012 Bern, Switzerland

b) School of Chemistry, University of Nottingham, University Park, Nottingham, NG7 2RD, UK

c) Organic Chemistry and Catalysis, Debye Institute for Materials Science, Faculty of Science, Utrecht University, 3584CG Utrecht, The Netherlands

* martin.albrecht@dcb.unibe.ch

Content:

1. Powder XRD

The powder X-Ray diffractogram of (**1**)Cu(OAc)$_2$ measured in transmission was calculated using cell parameters extracted from the reported crystal structure (Table S1)[1] and compared to the experimentally measured diffractogram (Table S2).

Table S1. Refined cell parameters for (**1**)Cu(OAc)$_2$.

Radiation wavelength	1.540598 nm
Cell_A	22.932(7) Å
Cell_B	8.706(3) Å
Cell_C	18.001(5) Å
Cell_Beta	119.369(23) Å
Cell_Volume	3131.9(28) Å

Table S2. Parameters of the measured (obs.) and the calculated (calc.) diffractogram for (**1**)Cu(OAc)$_2$.

2θ obs.	H K L	2θ calc.	|obs-calc|	d obs.	d calc.	Intensity
8.835	2 0 0	8.843	0.0073	10.0005	9.9922	100.0
10.368	-2 0 2	10.366	0.0019	8.5251	8.5267	21.1
11.090	1 1 0	11.077	0.0133	7.9718	7.9814	45.7
11.277	0 0 2	11.272	0.0052	7.8403	7.8439	39.8
13.382	1 1 1	13.385	0.0030	6.6111	6.6096	11.6
14.173	-1 1 2	14.185	0.0125	6.2440	6.2386	21.5
18.360	-1 1 3	18.357	0.0025	4.8284	4.8291	40.6
18.628	-3 1 3	18.627	0.0012	4.7594	4.7597	42.8
19.835	-2 0 4	19.837	0.0017	4.4725	4.4722	13.7
20.386	0 2 0	20.386	0.0001	4.3529	4.3529	21.6
21.158	0 2 1	21.165	0.0071	4.1958	4.1944	17.4
21.874	-2 2 1	21.861	0.0125	4.0600	4.0623	20.7
22.330	-3 1 4	22.331	0.0013	3.9781	3.9778	28.5
22.658	0 0 4	22.654	0.0044	3.9212	3.9219	40.0
23.323	-6 0 2	23.322	0.0011	3.8109	3.8111	18.5
25.817	-4 2 2	25.810	0.0071	3.4481	3.4490	20.9
26.742	6 0 0	26.744	0.0019	3.3310	3.3307	13.3
29.774	-4 0 6	29.776	0.0019	2.9983	2.9981	10.6

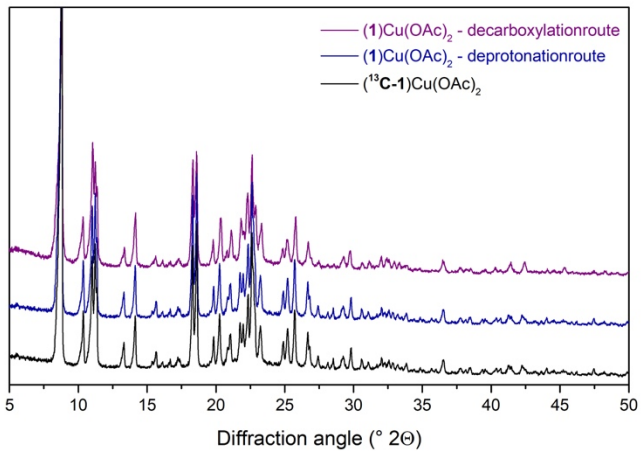

Figure S1. Powder X-Ray diffractograms of complexes (1)Cu(OAc)$_2$ synthesized following the deprotonation (blue) or decarboxylation (purple) route, and of complex (^{13}C-1)Cu(OAc)$_2$ (black).

2. Infrared spectra

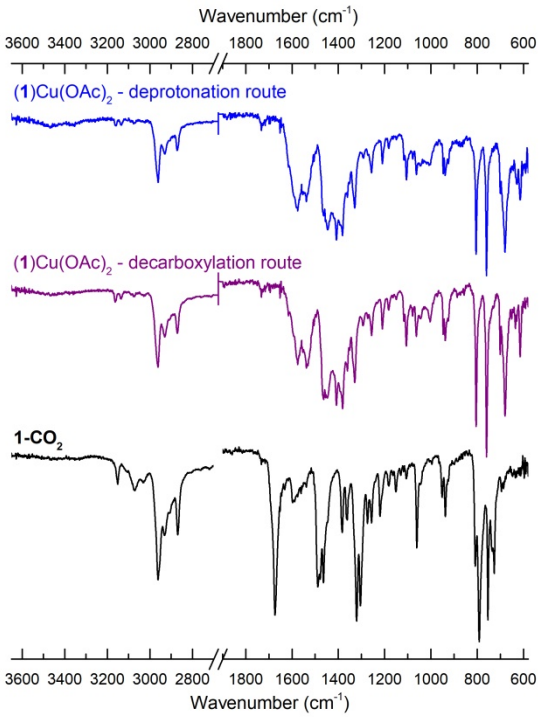

Figure S2. ATR-FTIR spectra of (**1**)$Cu(OAc)_2$ synthesized following the deprotonation (top) or decarboxylation (middle) route compared to the spectrum of **1-CO_2** (bottom), measured on solids.

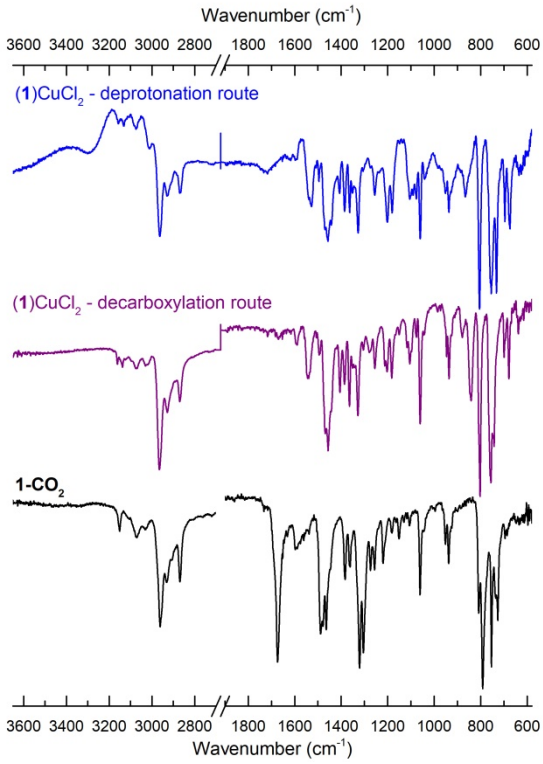

Figure S3. ATR-FTIR spectra of (**1**)$CuCl_2$ synthesized following the deprotonation (top) or decarboxylation (middle) route compared to the spectrum of **1-CO_2** (bottom), measured on solids.

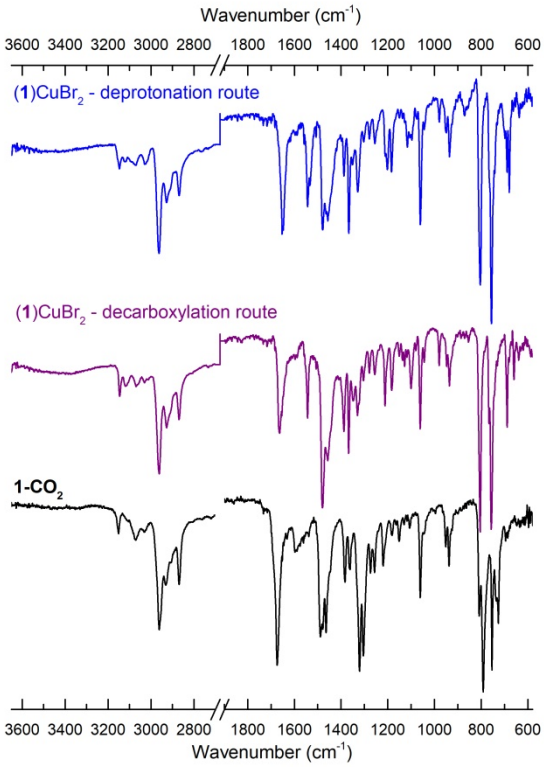

Figure S4. ATR-FTIR spectra of (**1**)$CuBr_2$ synthesized following the deprotonation (top) or decarboxylation (middle) route compared to the spectrum of **1-CO_2** (bottom), measured on solids.

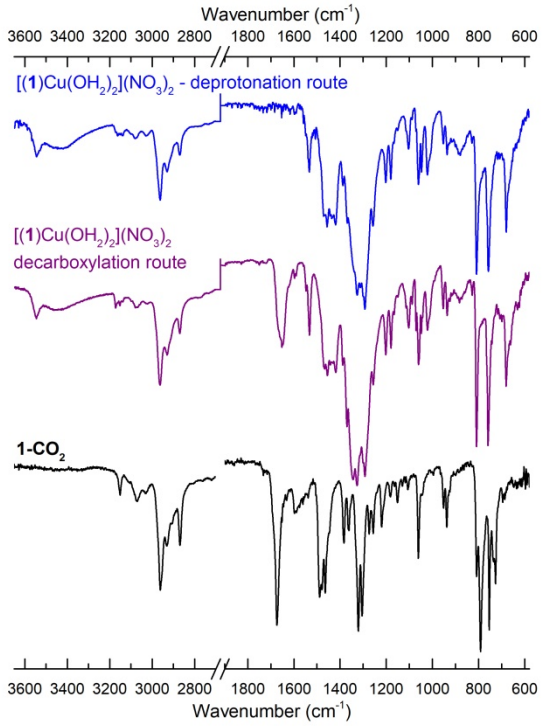

Figure S5. ATR-FTIR spectra of [(**1**)$Cu(OH_2)_2$]$(NO_3)_2$ synthesized following the deprotonation (top) or decarboxylation (middle) route compared to the spectrum of **1-CO_2** (bottom), measured on solids. Vibration band at 1650 cm^{-1} for DMF.

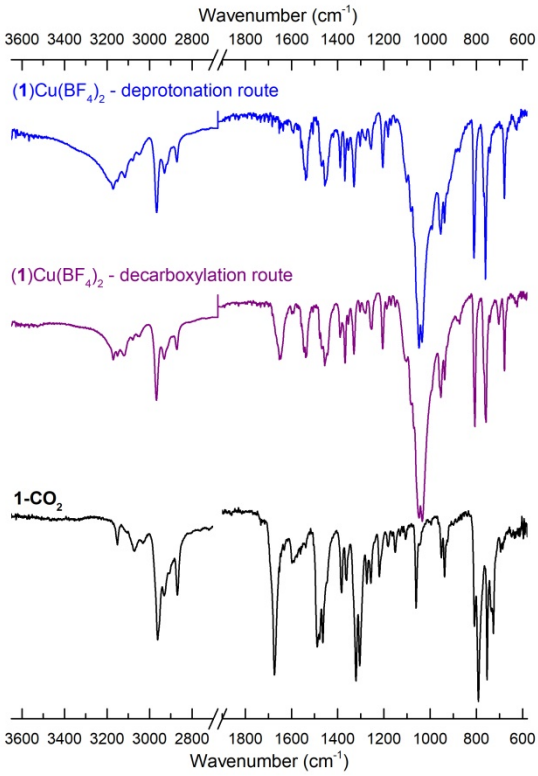

Figure S6. ATR-FTIR spectra of (**1**)$Cu(BF_4)_2$ synthesized following the deprotonation (top) or decarboxylation (middle) route compared to the spectrum of **1-CO_2** (bottom), measured on solids. Vibration band at 1650 cm^{-1} for DMF.

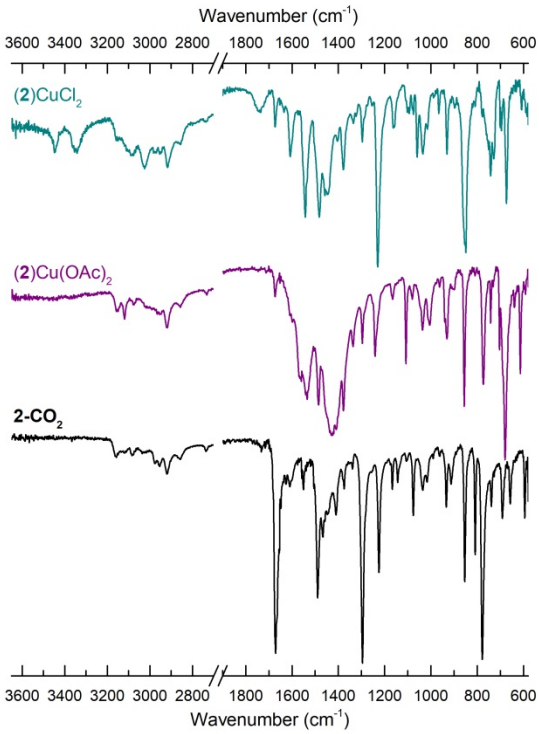

Figure S7. ATR-FTIR spectra of (**2**)$CuCl_2$ (top) and (**2**)$Cu(OAc)_2$ (middle) synthesized following the decarboxylation route and compared to the spectrum of **2-CO_2** (bottom), measured on solids.

3. Mass spectra

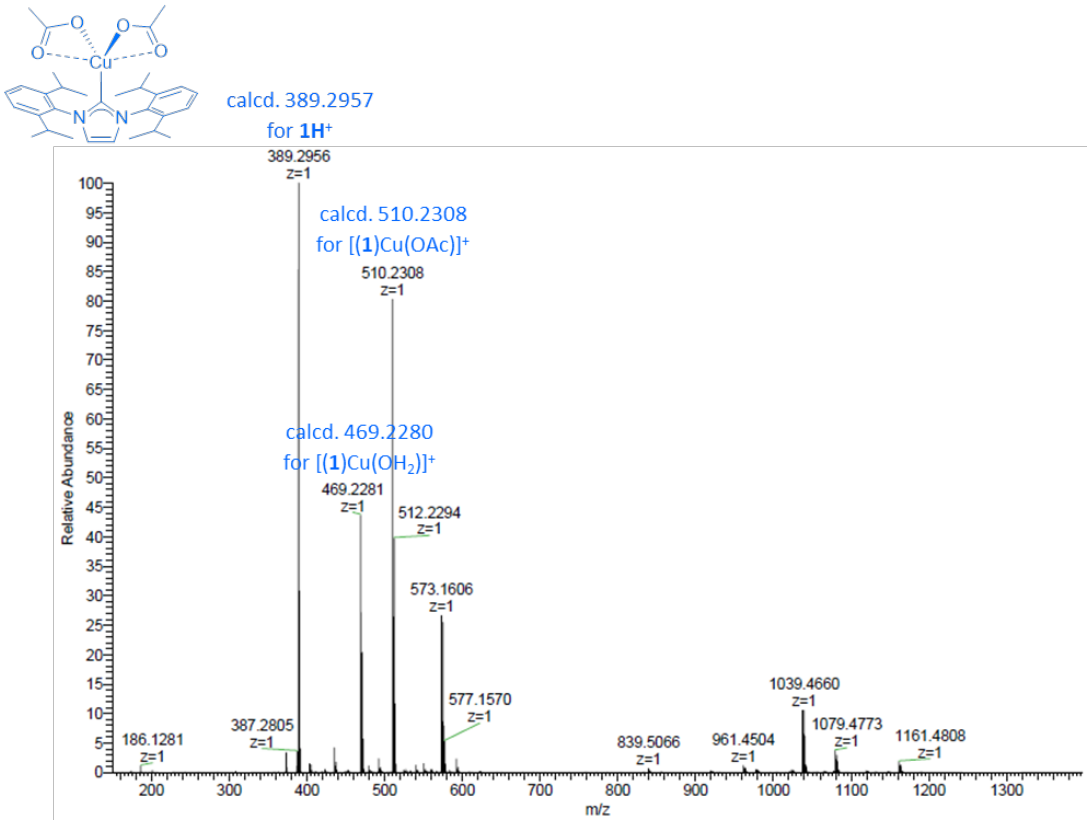

Figure S8. ESI-MS spectrum of (**1**)Cu(OAc)$_2$ freshly dissolved in acetonitrile, in positive mode.

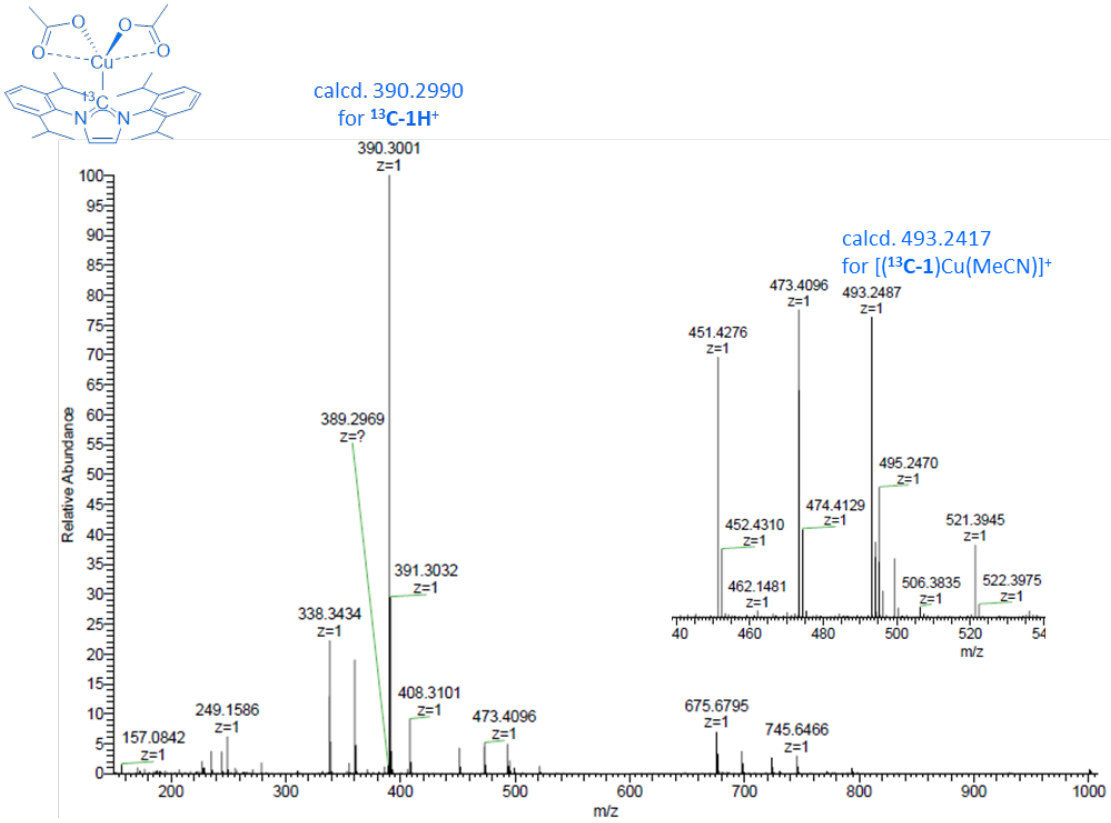

Figure S9. Selected area of the ESI-MS spectrum of (**^{13}C-1**)Cu(OAc)$_2$ freshly dissolved in acetonitrile, in positive mode.

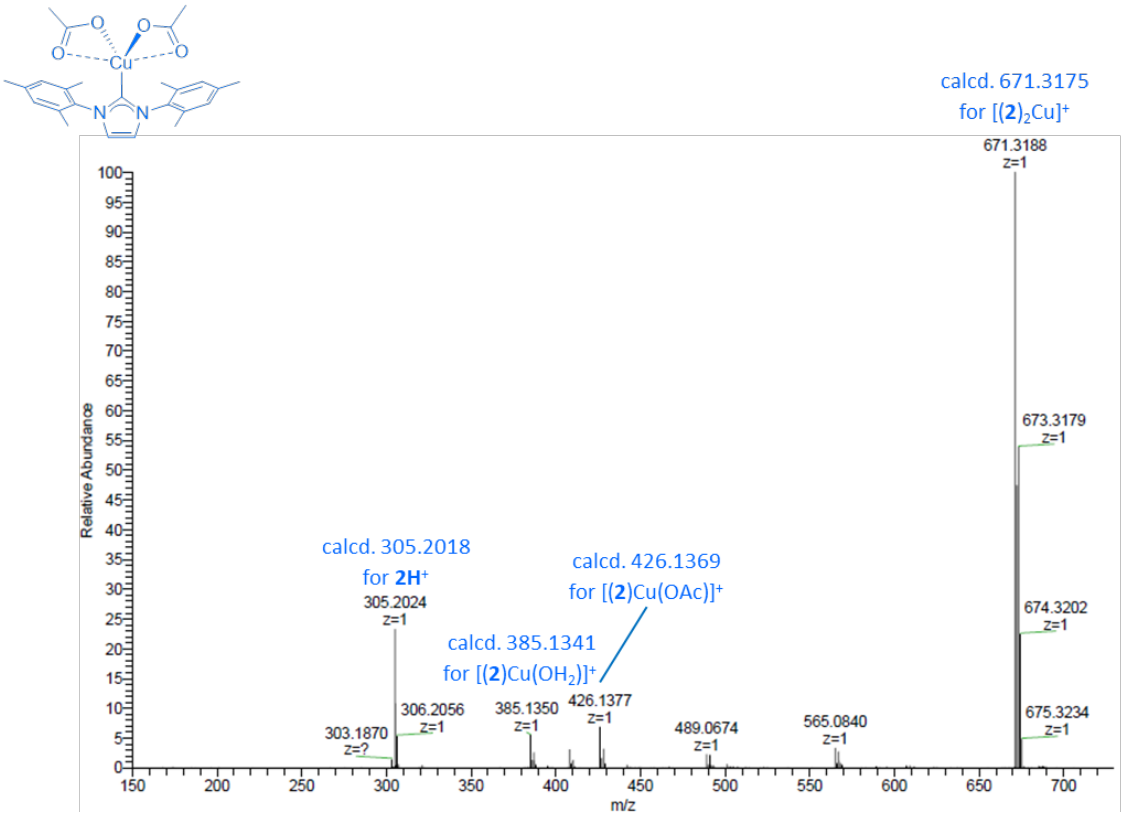

Figure S10. ESI-MS spectrum of (**2**)Cu(OAc)$_2$ prepared following the deprotonation route, freshly dissolved in acetonitrile, in positive mode.

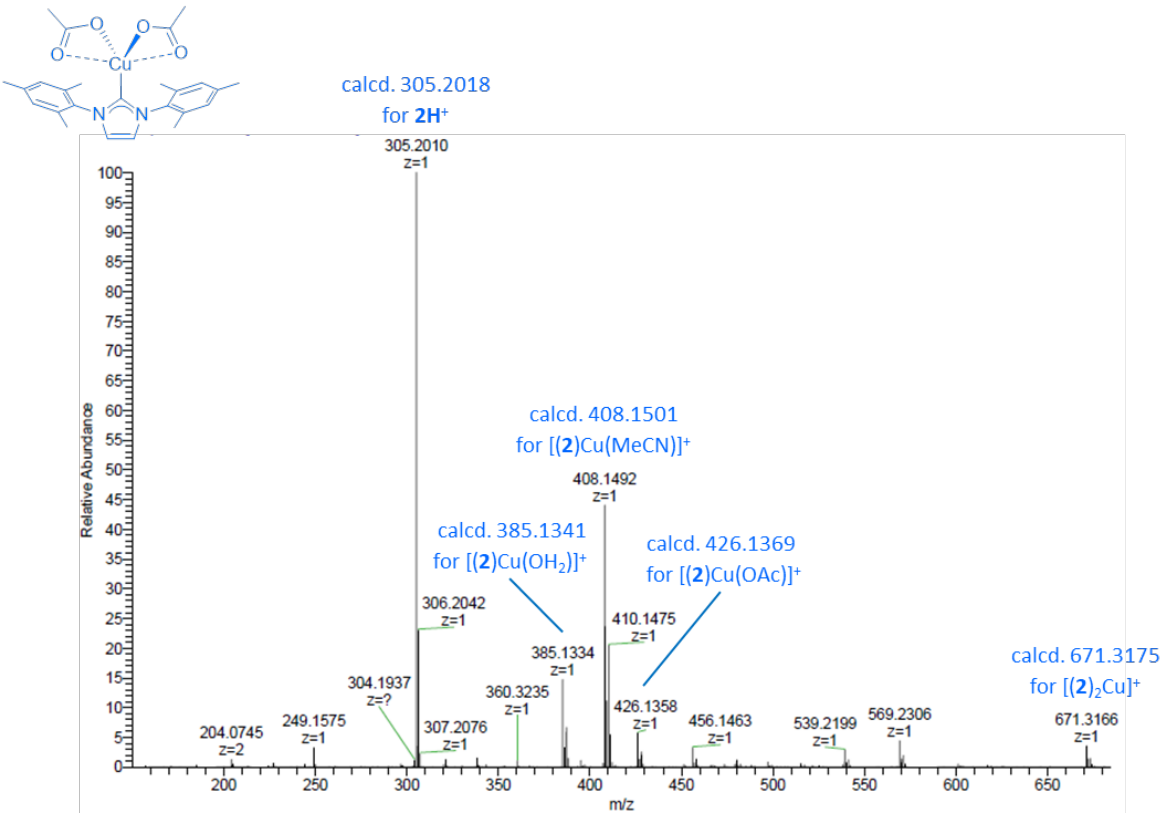

Figure S11. ESI-MS spectrum of (**2**)Cu(OAc)$_2$ prepared following the decarboxylation route, freshly dissolved in acetonitrile, in positive mode.

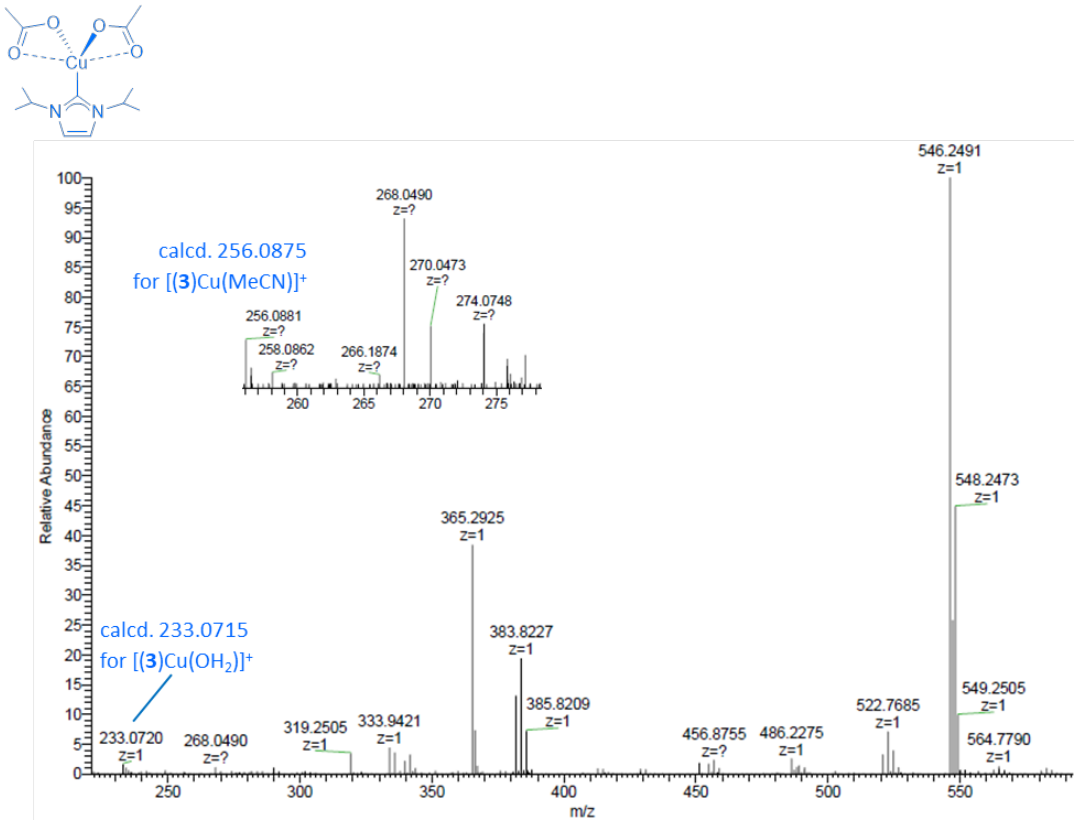

Figure S12. ESI-MS spectra of (**3**)Cu(OAc)$_2$ freshly dissolved in acetonitrile, in positive mode.

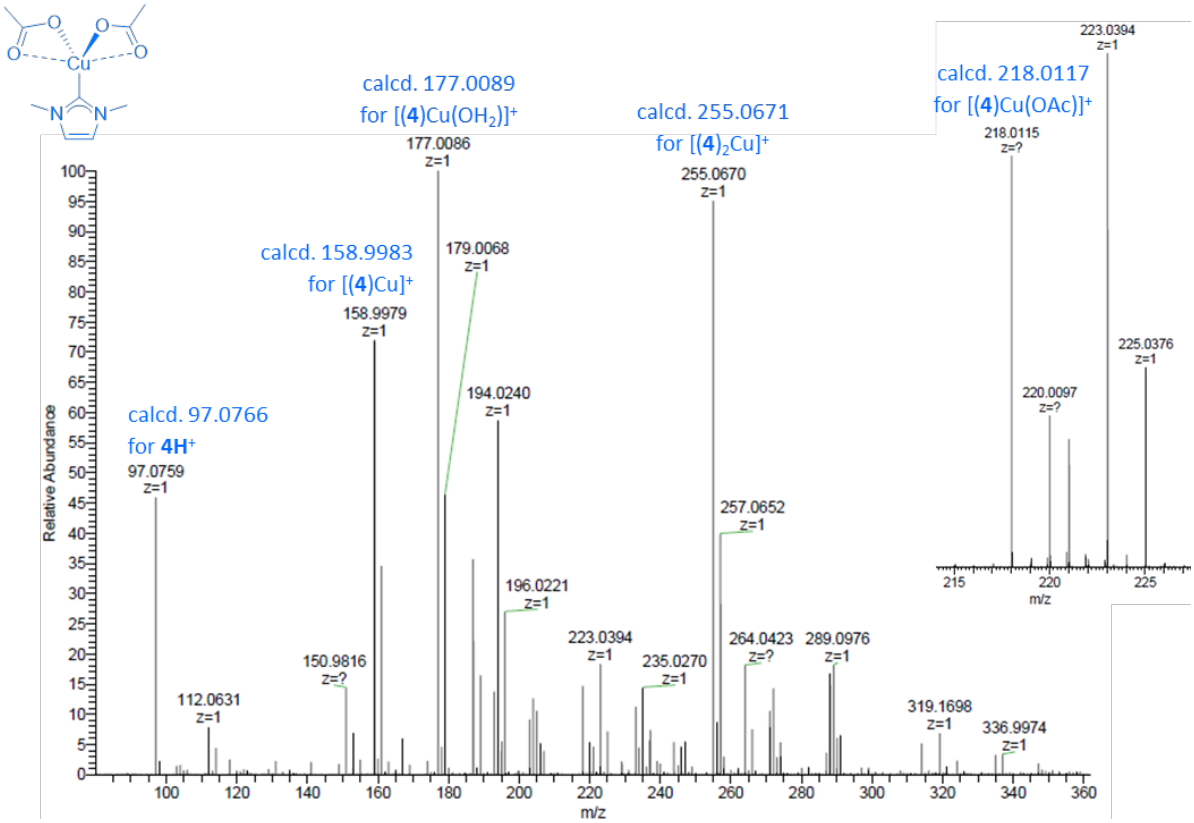

Figure S13. ESI-MS spectra of (**4**)Cu(OAc)$_2$ freshly dissolved in acetonitrile, in positive mode.

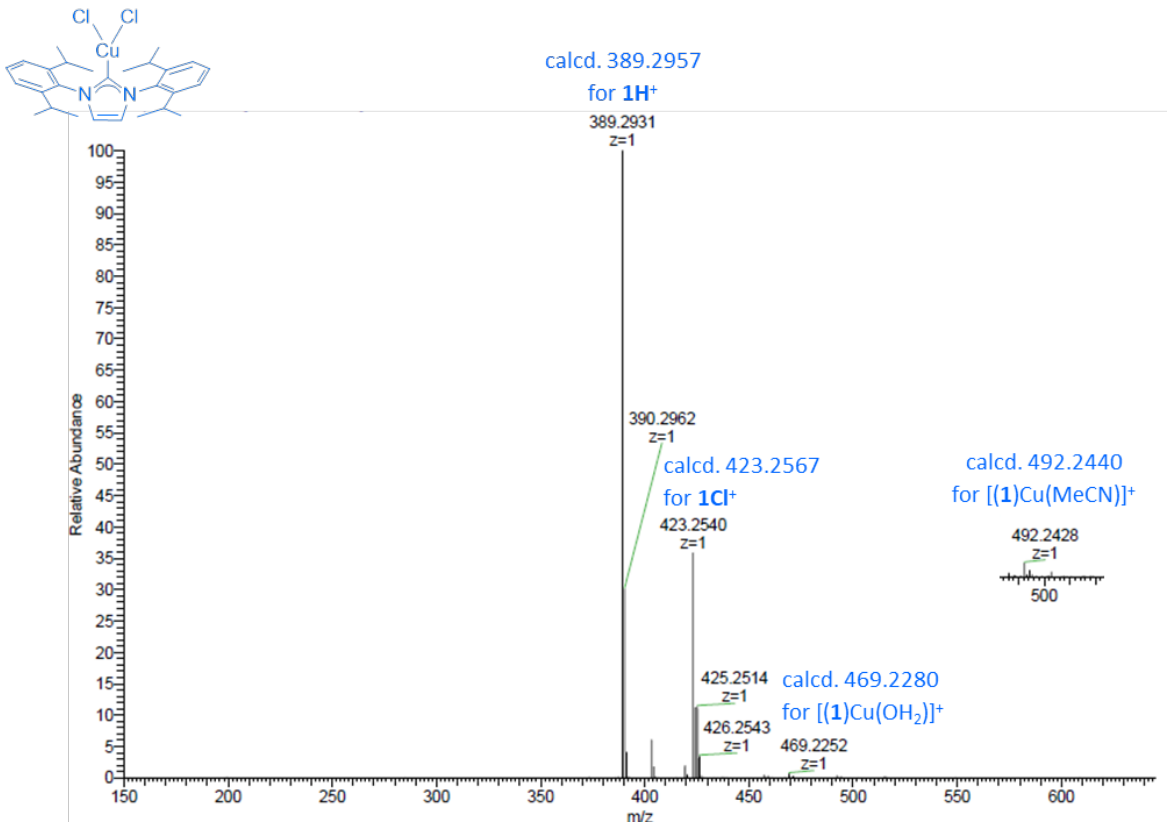

Figure S14. ESI-MS spectra of (**1**)$CuCl_2$ freshly dissolved in acetonitrile, in positive mode.

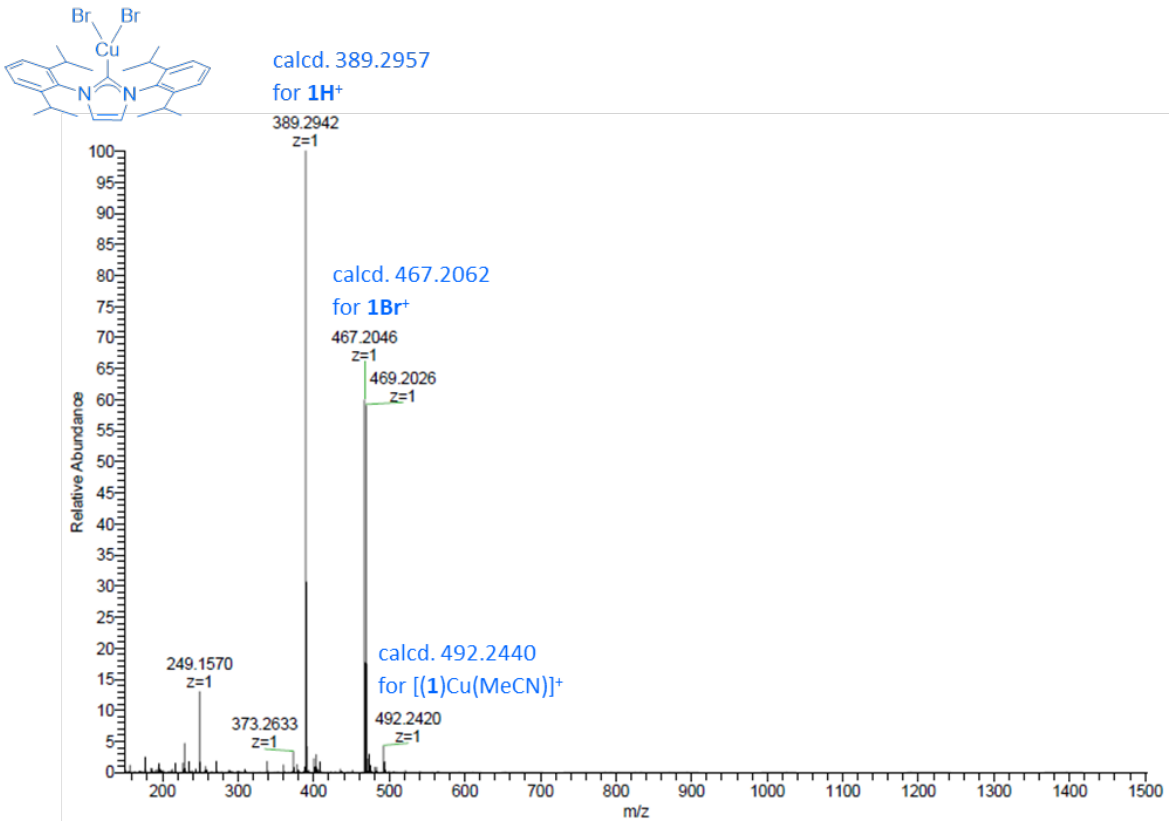

Figure S15. ESI-MS spectra of (**1**)$CuBr_2$ freshly dissolved in acetonitrile, in positive mode.

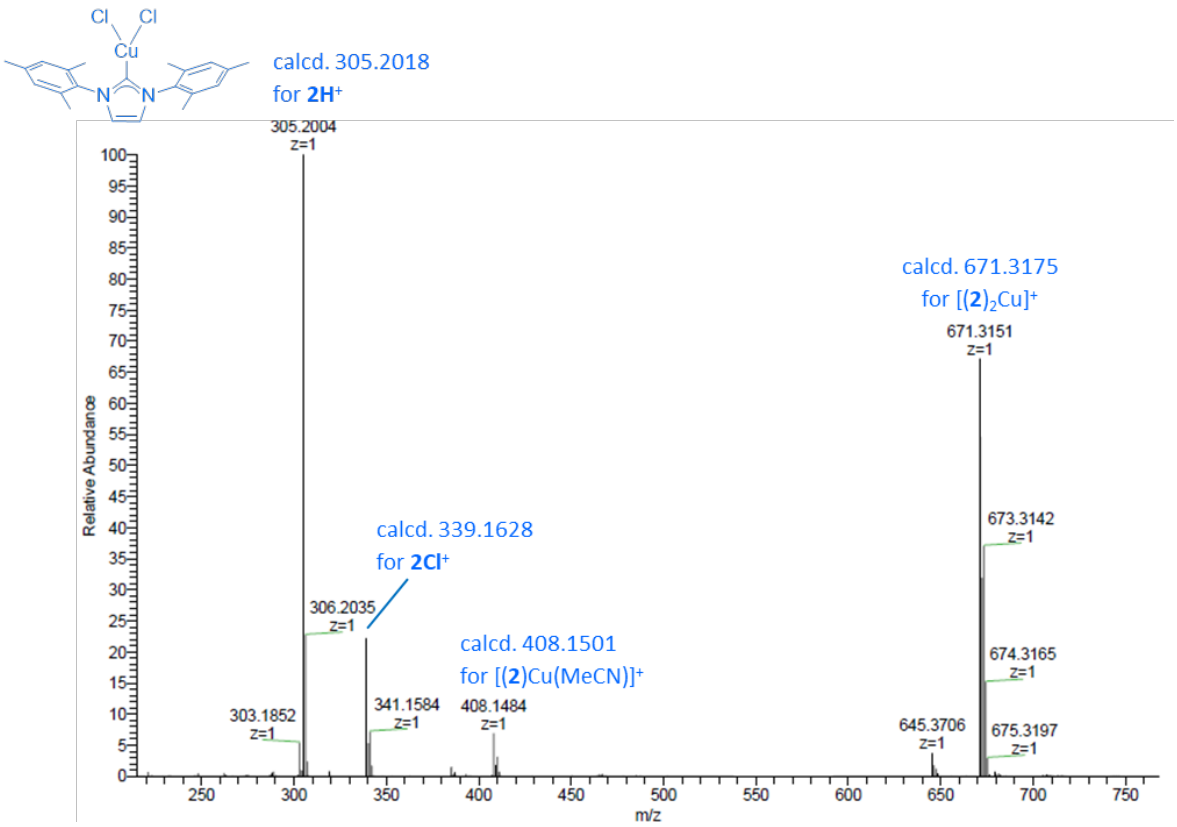

Figure S16. ESI-MS spectra of (**2**)$CuCl_2$ freshly dissolved in acetonitrile, in positive mode.

4. EPR spectra

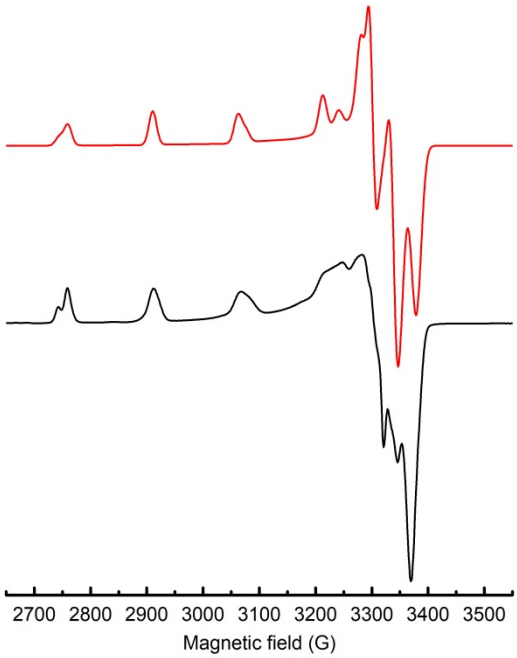

Figure S17. X-band EPR spectra at 77 K of (**1**)Cu(OAc)$_2$ in CH_2Cl_2:toluene (1:9) (black line) and simulated (red line) as a mixture of 2 species with parameters: species 1, $g_{1,2,3}$ = 2.27, 2.057, 2.030; A(^{63}Cu)$_{1,2,3}$ (× 10^{-4} cm^{-1}) = 160, 0, 0; linewidth$_{1,2,3}$ = 50, 40, 50 MHz; species 2 = 0.7 * species 1, $g_{1,2,3}$ = 2.265, 2.057, 2.030; A(^{63}Cu)$_{1,2,3}$ (× 10^{-4} cm^{-1}) = 175, 0, 0; linewidth$_{1,2,3}$ = 50, 40, 50 MHz.

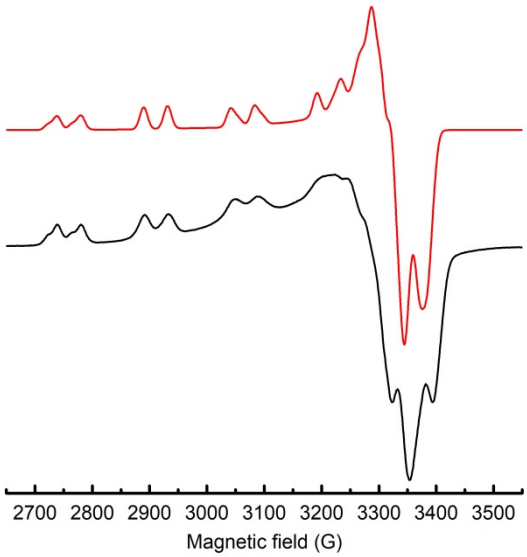

Figure S18. X-band EPR spectra at 77 K of (**^{13}C-1**)Cu(OAc)$_2$ in CH_2Cl_2:toluene (1:9) (black line) and simulated (red line) as a mixture of 2 species with parameters: species 1, $g_{1,2,3}$ = 2.27, 2.057, 2.030; A(^{63}Cu)$_{1,2,3}$ (× 10^{-4} cm^{-1}) = 160, 0, 0; a(^{13}C)$_{1,2,3}$ (× 10^{-4} cm^{-1}) = 44, 15, 0; linewidth$_{1,2,3}$ = 50, 40, 50 MHz; species 2 = 0.7 * species 1, $g_{1,2,3}$ = 2.265, 2.057, 2.030; A(^{63}Cu)$_{1,2,3}$ (× 10^{-4} cm^{-1}) = 175, 0, 0; a(^{13}C)$_{1,2,3}$ (× 10^{-4} cm^{-1}) = 44, 15, 0; linewidth$_{1,2,3}$ = 50, 40, 50 MHz.

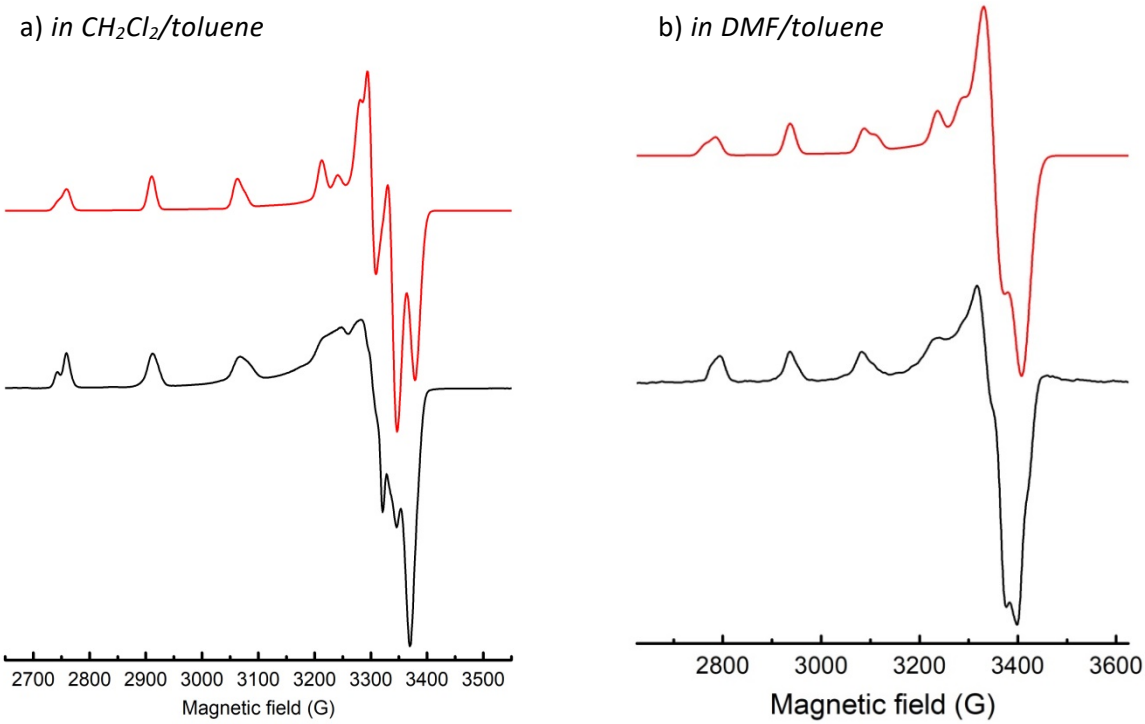

Figure S19. X-band EPR spectra at 77 K of (**1**)$Cu(OAc)_2$ in CH_2Cl_2:toluene (1:9) (black line) and simulated (red line) as a mixture of 2 species with parameters: species 1, $g_{1,2,3}$ = 2.27, 2.057, 2.030; $A(^{63}Cu)_{1,2,3}$ (× 10^{-4} cm^{-1}) = 160, 0, 0; $linewidth_{1,2,3}$ = 50, 40, 50 MHz; species 2 = 0.7 * species 1, $g_{1,2,3}$ = 2.265, 2.057, 2.030; $A(^{63}Cu)_{1,2,3}$ (× 10^{-4} cm^{-1}) = 175, 0, 0; $linewidth_{1,2,3}$ = 50, 40, 50 MHz; and b) (**1**)$Cu(OAc)_2$ in DMF:toluene (1:9) (black line) and simulated (red line) as a mixture of 2 species with parameters: species 1, $g_{1,2,3}$ = 2.29, 2.055, 2.055; $A(^{63}Cu)_{1,2,3}$ (× 10^{-4} cm^{-1}) = 160, 0, 0; $linewidth_{1,2,3}$ = 80, 120, 120 MHz; species 2 = 0.6 * species 1, $g_{1,2,3}$ = 2.28, 2.055, 2.055; $A(^{63}Cu)_{1,2,3}$ (× 10^{-4} cm^{-1}) = 185, 0, 0; $linewidth_{1,2,3}$ = 80, 120, 120 MHz.

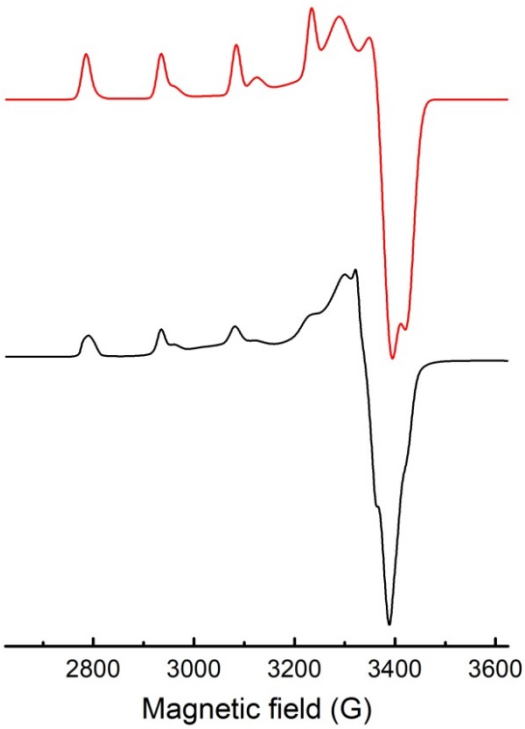

Figure S20. X-band EPR spectra at 77 K of (**2**)$Cu(OAc)_2$ in DMF:toluene (1:9) (black line) and simulated (red line) as a mixture of 2 species with parameters: species 1, $g_{1,2,3}$ = 2.29, 2.075, 2.035; $A(^{63}Cu)_{1,2,3}$ (× 10^{-4} cm^{-1}) = 160, 20, 0; $linewidth_{1,2,3}$ = 60, 140, 80 MHz; species 2 = 0.4 * species 1, $g_{1,2,3}$ = 2.266, 2.075, 2.035; $A(^{63}Cu)_{1,2,3}$ (× 10^{-4} cm^{-1}) = 175, 20, 0; $linewidth_{1,2,3}$ = 100, 140, 80 MHz.

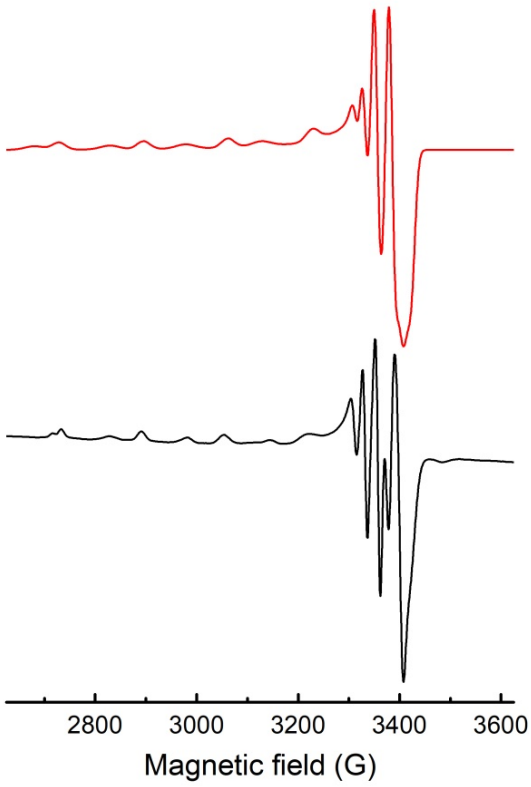

Figure S21. X-band EPR spectra at 77 K of (**3**)Cu(OAc)$_2$ in DMF:toluene (1:9) (black line) and simulated (red line) as a mixture of 2 species with parameters: species 1, $g_{1,2,3}$ = 2.375, 2.058, 2.038; A(^{63}Cu)$_{1,2,3}$ (× 10^{-4} cm^{-1}) = 165, 20, 0; linewidth$_{1,2,3}$ = 150, 40, 40 MHz; species 2 = 1.2 * species 1, $g_{1,2,3}$ = 2.315, 2.058, 2.038; A(^{63}Cu)$_{1,2,3}$ (× 10^{-4} cm^{-1}) = 180, 20, 0; linewidth$_{1,2,3}$ = 100, 40, 40 MHz.

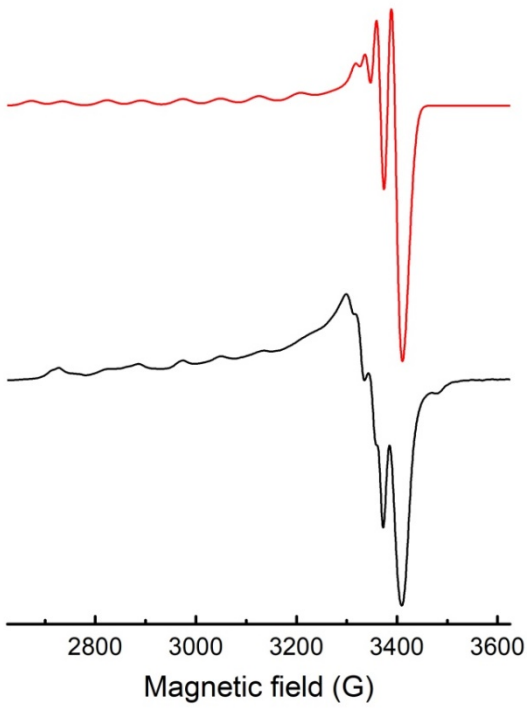

Figure S22. X-band EPR spectra at 77 K of (**4**)Cu(OAc)$_2$ in DMF:toluene (1:9) (black line) and simulated (red line) as a mixture of 2 species with parameters: species 1, $g_{1,2,3}$ = 2.378, 2.05, 2.035; A(^{63}Cu)$_{1,2,3}$ (× 10^{-4} cm^{-1}) = 167, 20, 0; linewidth$_{1,2,3}$ = 130, 50, 70 MHz; species 2 = 0.8 * species 1, $g_{1,2,3}$ = 2.321, 2.05, 2.035; A(^{63}Cu)$_{1,2,3}$ (× 10^{-4} cm^{-1}) = 170, 20, 0; linewidth$_{1,2,3}$ = 130, 150, 70 MHz.

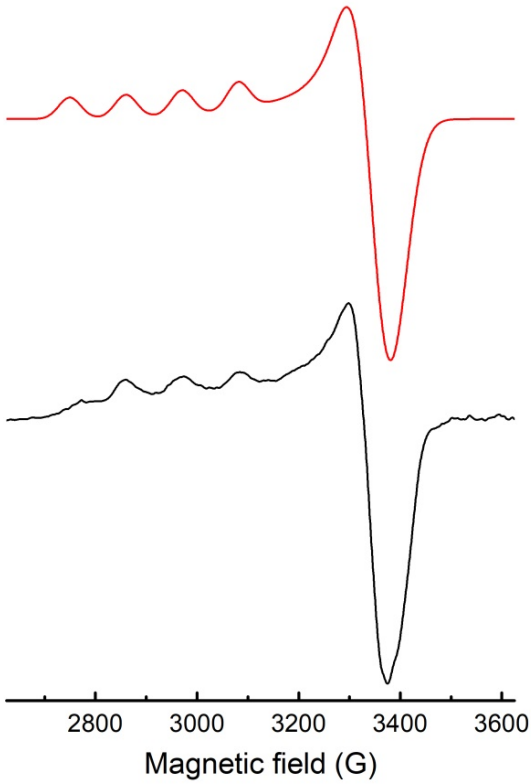

Figure S23. X-band EPR spectra at 77 K of (**1**)$CuCl_2$ in DMF:toluene (1:9) (black line) and simulated (red line) with parameters: $g_{1,2,3}$ = 2.365, 2.072, 2.043; $A(^{63}Cu)_{1,2,3}$ (× 10^{-4} cm^{-1}) = 122, 0, 0; $linewidth_{1,2,3}$ = 170, 225, 225 MHz.

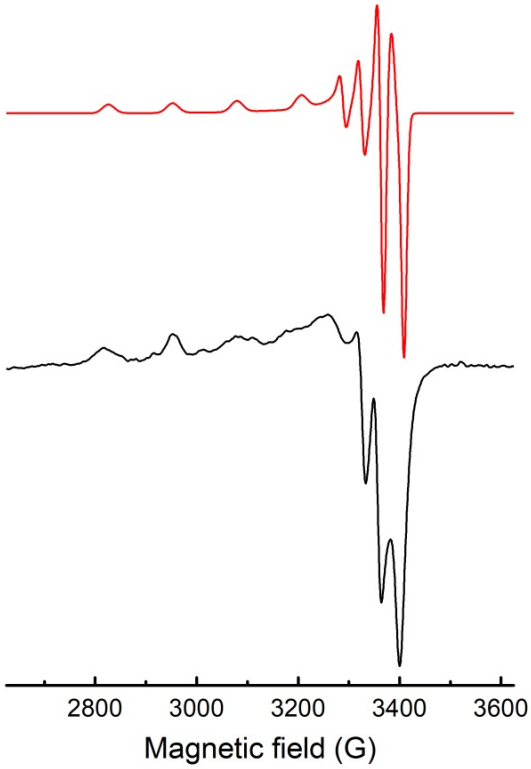

Figure S24. X-band EPR spectra at 77 K of (**1**)$Cu(NO_3)_2$ in DMF:toluene (1:9) (black line) and simulated (red line) with parameters: $g_{1,2,3}$ = 2.285, 2.057, 2.05; $A(^{63}Cu)_{1,2,3}$ (× 10^{-4} cm^{-1}) = 135, 38, 0; $linewidth_{1,2,3}$ = 90, 35, 50 MHz.

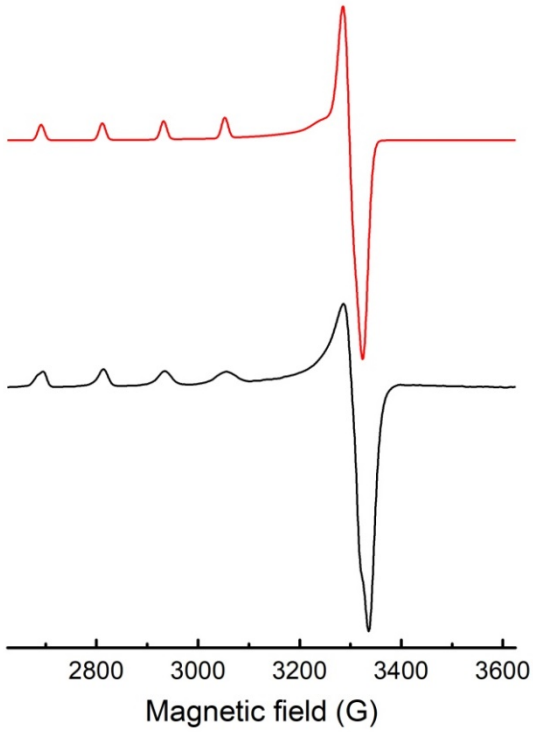

Figure S25. X-band EPR spectra at 77 K of (**1**)$Cu(OTf)_2$ in DMF:toluene (1:9) (black line) and simulated (red line) with parameters: $g_{1,2,3}$ = 2.4, 2.088, 2.088; $A(^{63}Cu)_{1,2,3}$ (× 10^{-4} cm^{-1}) = 135, 0, 0; $linewidth_{1,2,3}$ = 50, 70, 70 MHz.

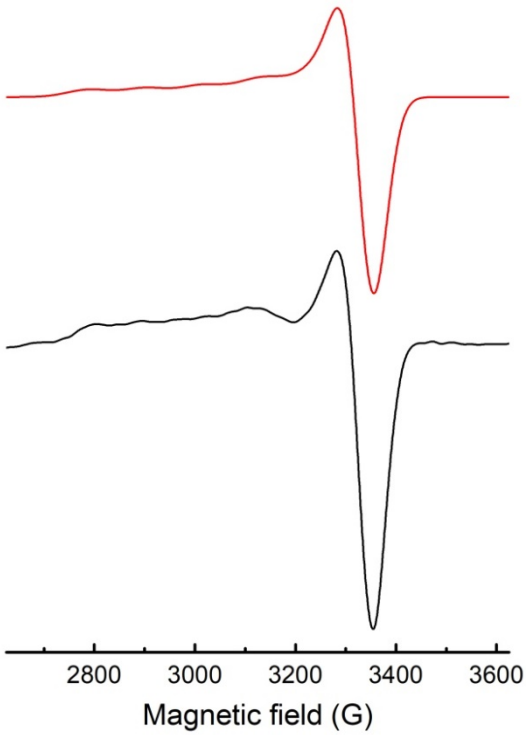

Figure S26. X-band EPR spectra at 77 K of (**2**)$CuCl_2$ in DMF:toluene (1:9) (black line) and simulated (red line) with parameters: $g_{1,2,3}$ = 2.33, 2.079, 2.06; $A(^{63}Cu)_{1,2,3}$ (× 10^{-4} cm^{-1}) = 122, 0, 0; $linewidth_{1,2,3}$ = 330, 200, 180 MHz.

5. NMR spectra

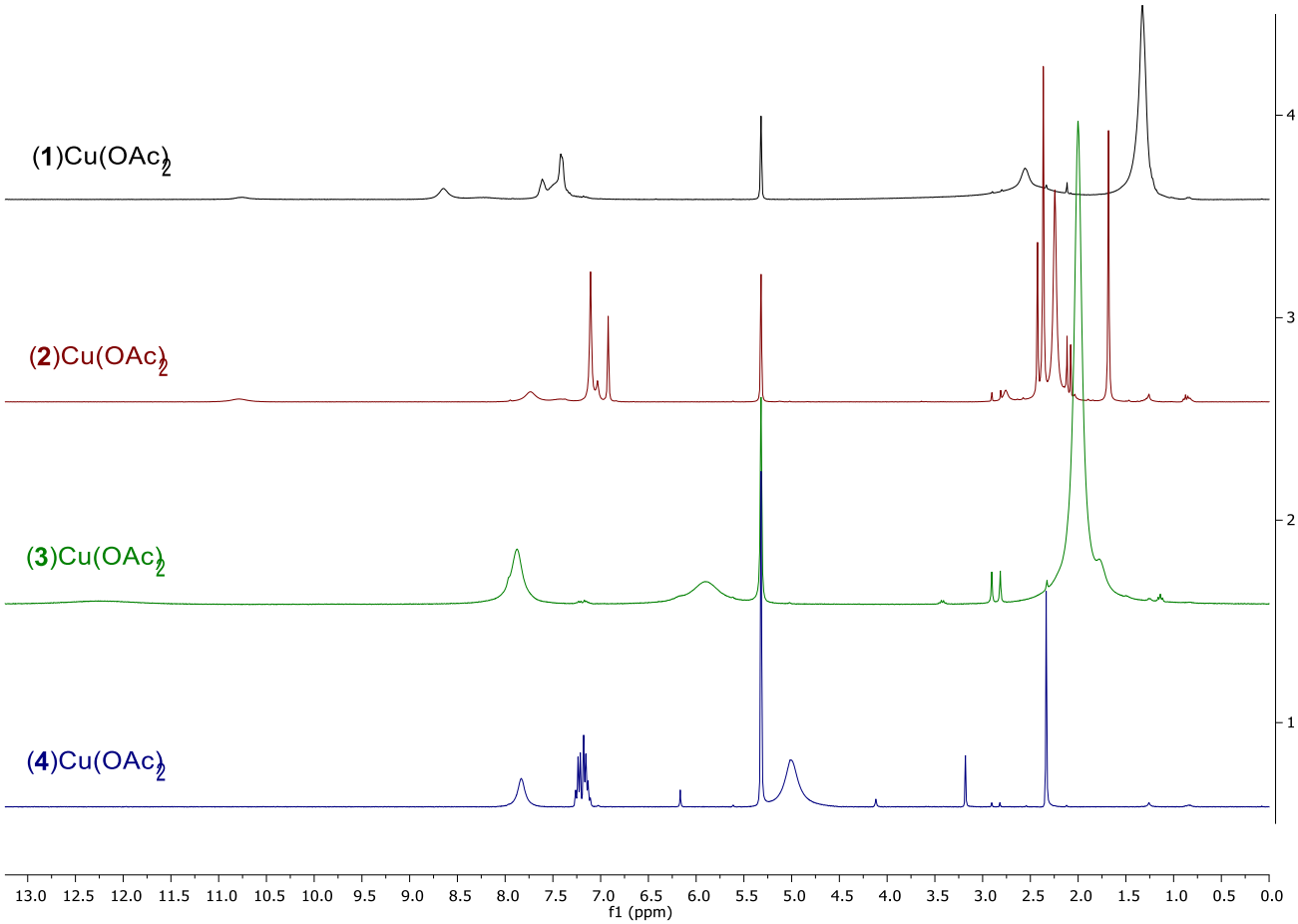

Figure S27. ^{1}H NMR spectra of complexes (NHC)Cu(OAc)$_2$ in CD_2Cl_2. Complex (**3**)Cu(OAc)$_2$ contains DMF and (**4**)Cu(OAc)$_2$ contains toluene.

The ^{1}H 2D DOSY experiment on a CD_2Cl_2 solution of crystals of (**1**)Cu(OAc)$_2$ on the 400 MHz spectrometer provides a 1D spectrum displaying sharp peaks compared to a simple 1H 1D experiment, with the broad peak at 10.5 ppm missing (see Figure S12). The 2D map is plotted based on intensity fitting of 9 selected peaks (Figure S13) and the different diffusion coefficients are extracted from the fitted curves (Table S3). A set of peaks at 0.91, 1.27 and 1.33 ppm attributed to pentane are observed on the 1D spectrum, however with diffusion coefficients ranging from 2.67 to 5.83 x 10^{-11} m^2/s. The signal at 2.15 ppm is assigned to acetate and has a diffusion coefficient of 5.18 x 10^{-11} m^2/s. The other peaks are assigned to the ligands and their diffusion coefficients span from 1.92 to 2.35 x 10^{-11} m^2/s. While one expects same diffusion coefficients for peaks assigned to the same compound, we observed a broad span for pentane and the ligand. The difference in diffusion coefficients for the ligand and acetate signals may be explained by ligand dissociation that can happen in solution, which has been observed using different ligands (see crystal structures obtained from complexes (**2**)Cu(OAc)$_2$, (**3**)Cu(OAc)$_2$ and (**4**)Cu(OAc)$_2$).

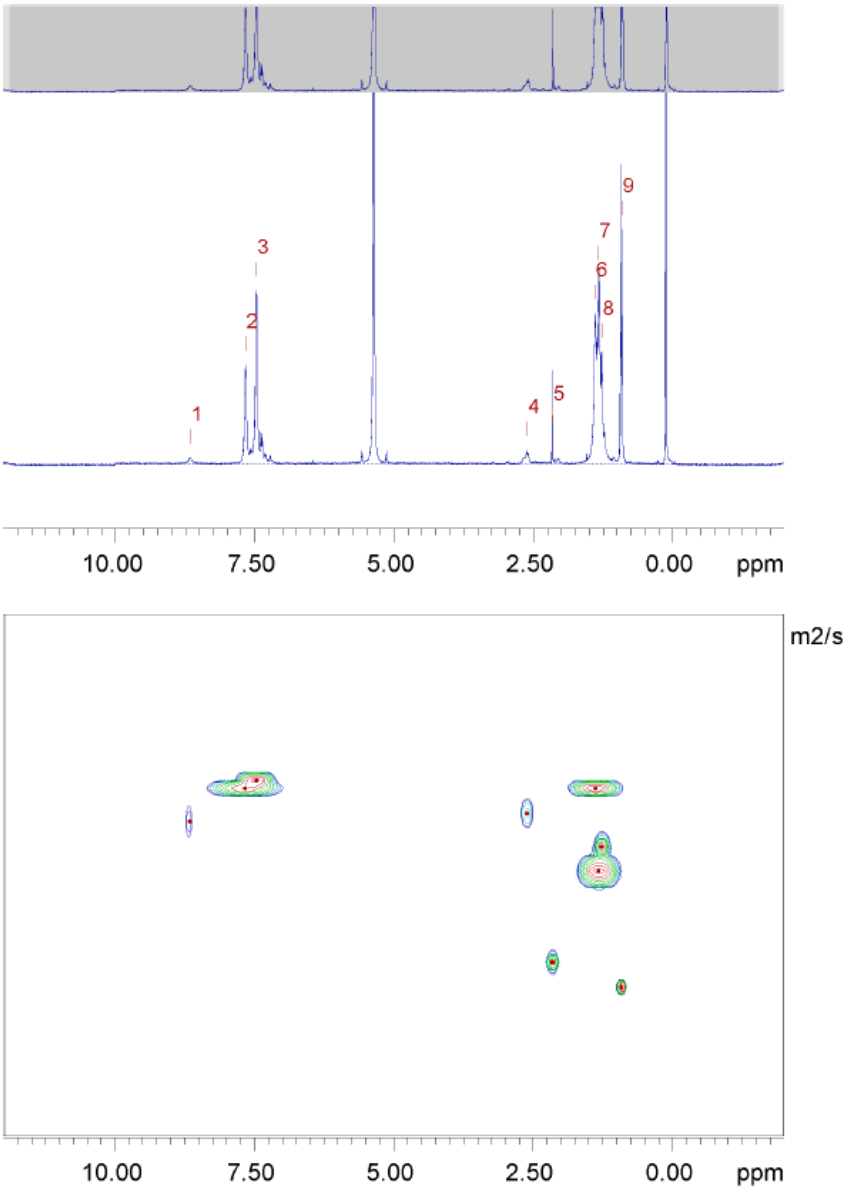

Figure S28. ^{1}H 2D DOSY spectrum (top) and DOSY plot based on fit (bottom) of 0.5 M (**1**)Cu(OAc)$_2$ in CD_2Cl_2, measured on 400 MHz spectrometer.

Table S3. Shifts and diffusion coefficients for selected peaks and their proposed assignment.

Peak name	F2 [ppm]	D [m^2/s]	error	Assignment
3	7.47	1.910E-11	3.194E-13	CH_{arom} **1**
2	7.66	1.939E-11	2.921E-13	CH_{arom} **1**
6	1.39	1.989E-11	2.323E-13	CH_3 **1**
4	2.61	2.224E-11	1.395E-12	$CH_{isopropyl}$ **1**
1	8.66	2.348E-11	2.474E-12	**1**
8	1.27	2.676E-11	8.311E-13	*Pentane*
7	1.33	3.145E-11	1.420E-12	*Pentane*
5	2.15	5.179E-11	1.410E-12	CH_3 acetate
9	0.91	5.833E-11	1.241E-12	*Pentane*

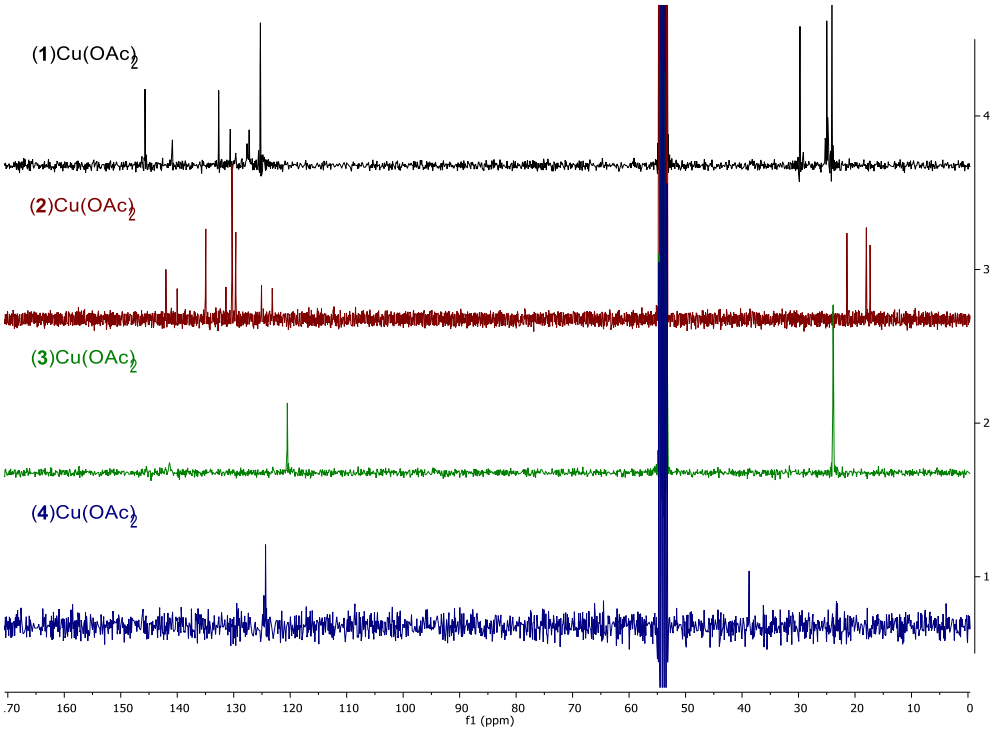

Figure S29. ^{13}C NMR spectra of complexes (NHC)Cu(OAc)$_2$ in CD_2Cl_2. Complex (**3**)Cu(OAc)$_2$ contains DMF and (**4**)Cu(OAc)$_2$ contains toluene.

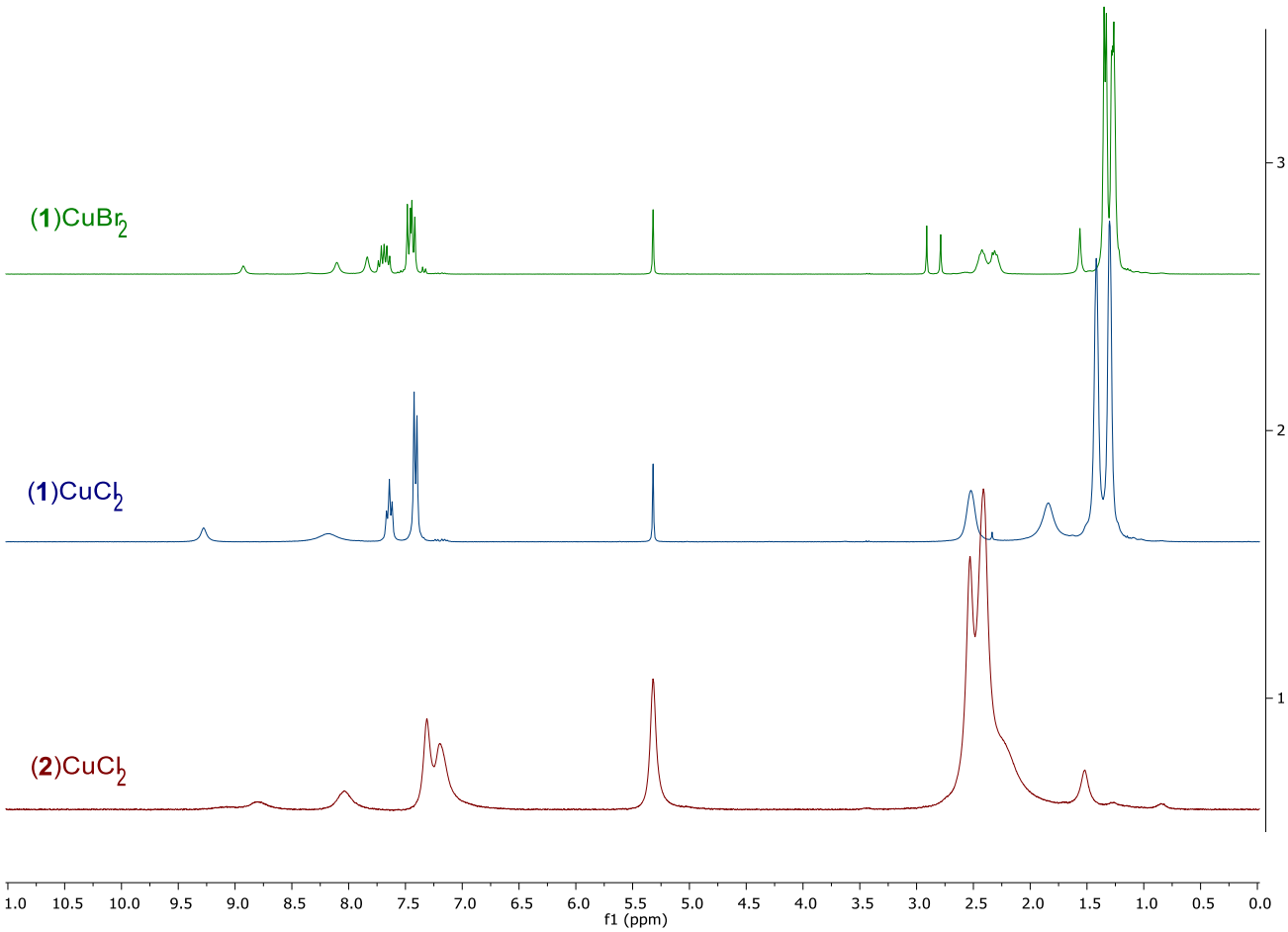

Figure S30. ^{1}H-NMR spectra of complexes (**1**)$CuCl_2$, (**1**)$CuBr_2$ and (**2**)$CuCl_2$ in CD_2Cl_2.

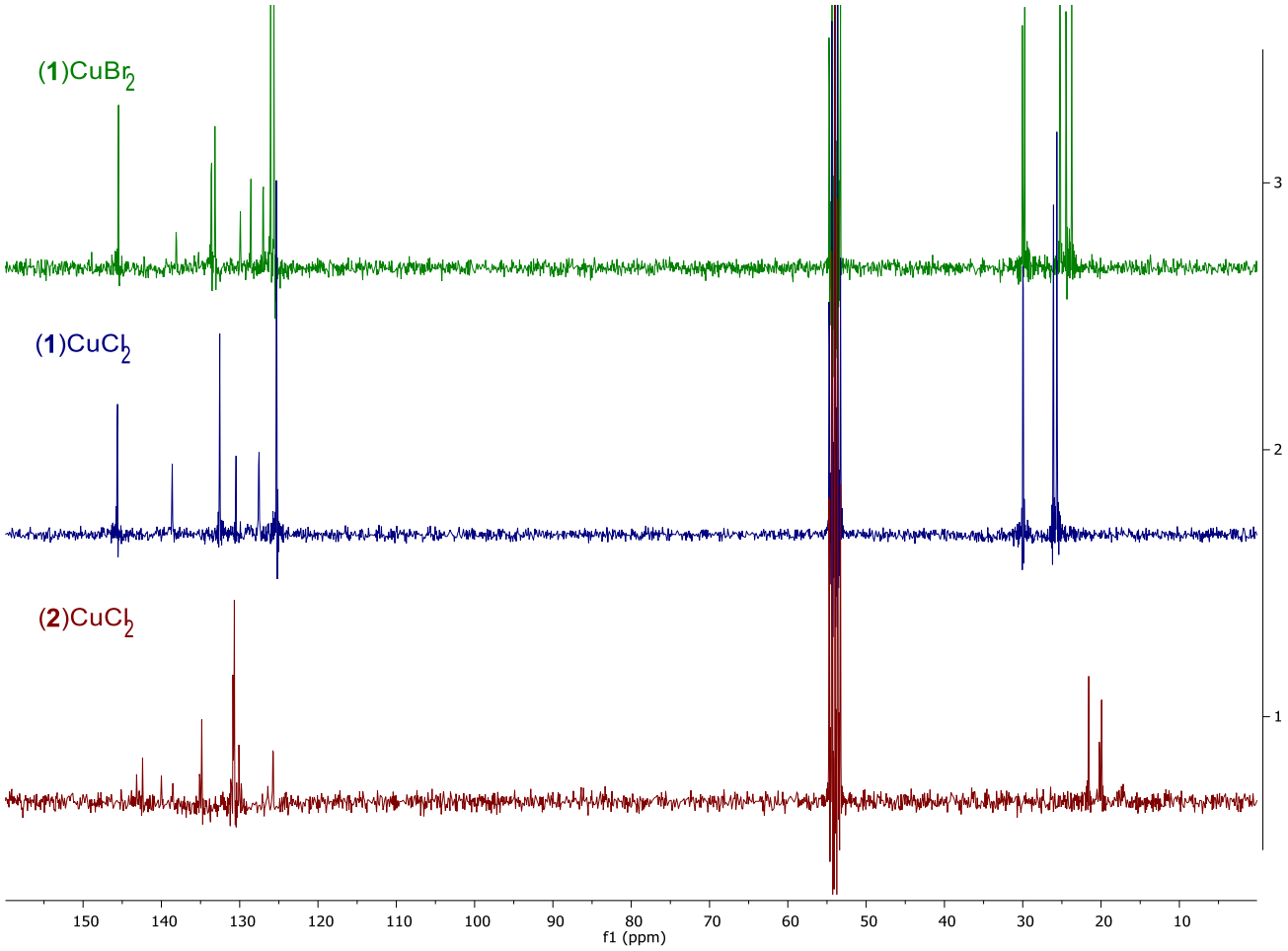

Figure S31. ^{13}C-NMR spectra of complexes (**1**)$CuCl_2$, (**1**)$CuBr_2$ and (**2**)$CuCl_2$ in CD_2Cl_2.

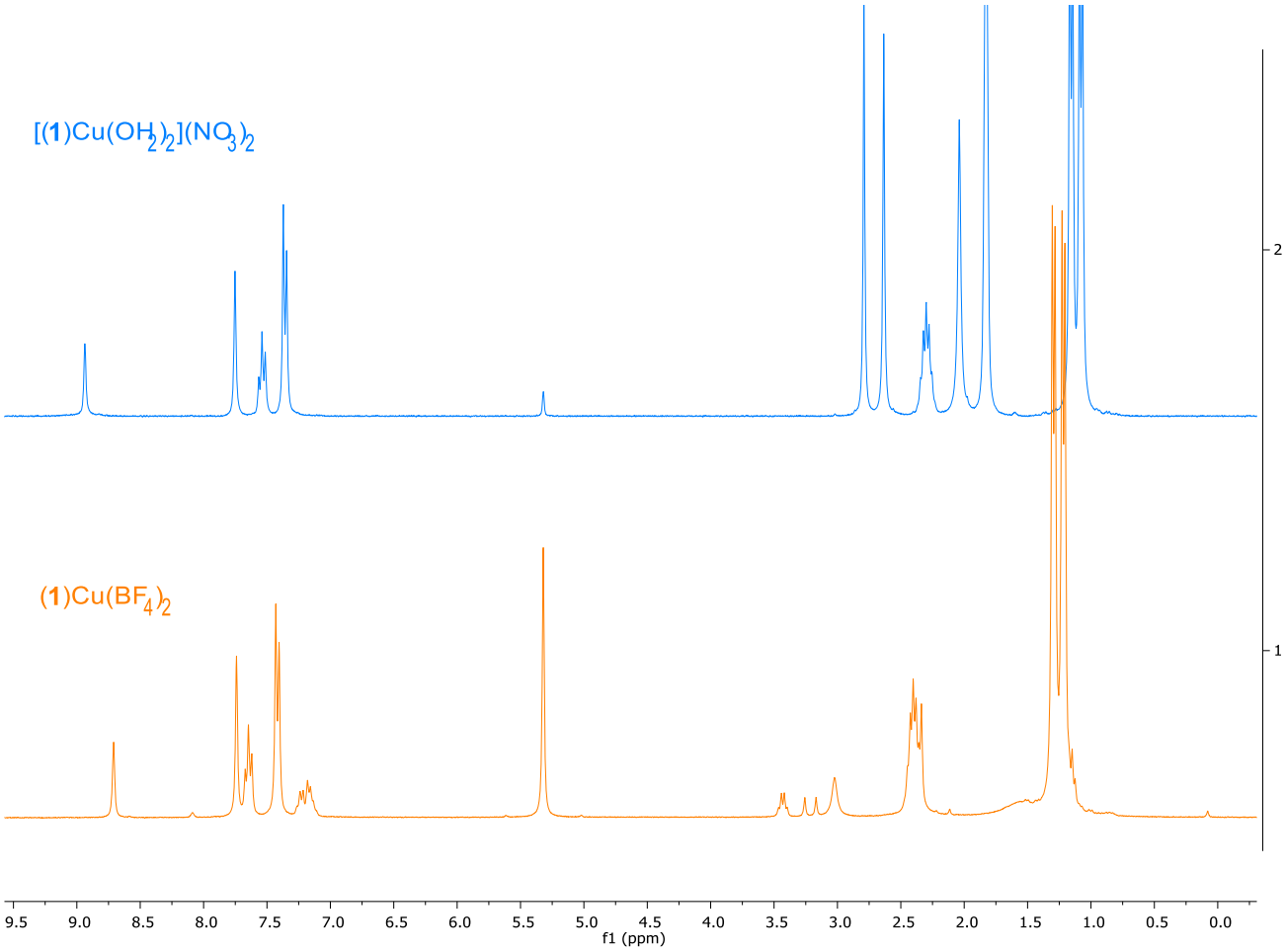

Figure S32. ^{1}H-NMR spectra of complexes [(**1**)Cu$(OH_2)_2$]$(NO_3)_2$ and (**1**)Cu$(BF_4)_2$ in CD_2Cl_2.

6. X-Ray structures

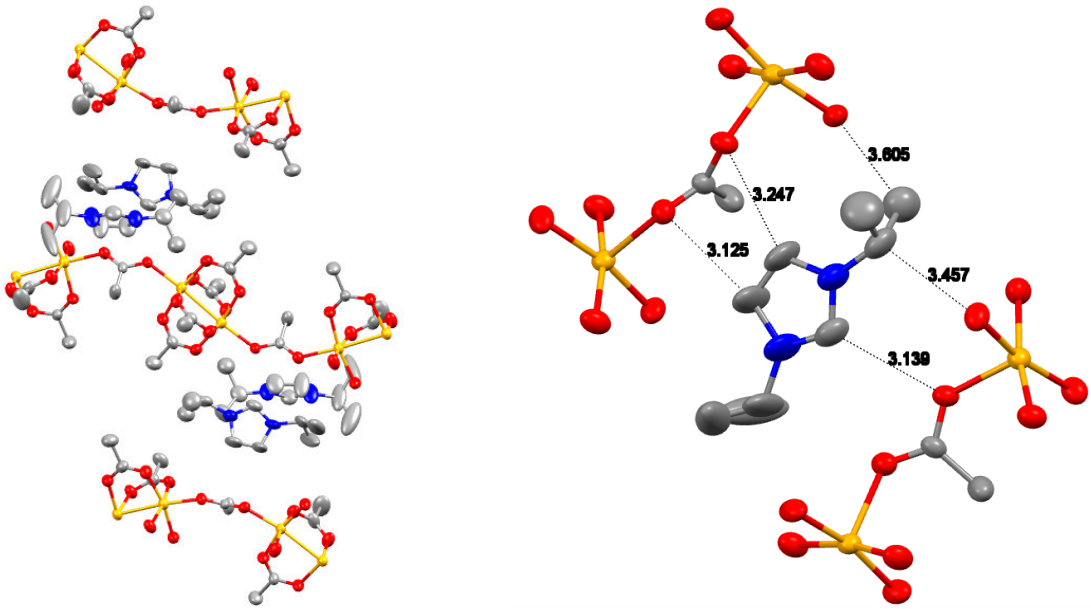

Figure S33. ORTEP representation of the packing of (**3H**)[$Cu_2(OAc)_5$] (left) and selected atom distances (right). All ellipsoids at 50% probability level; copper atoms in orange; hydrogen atoms and solvent molecules omitted for clarity.

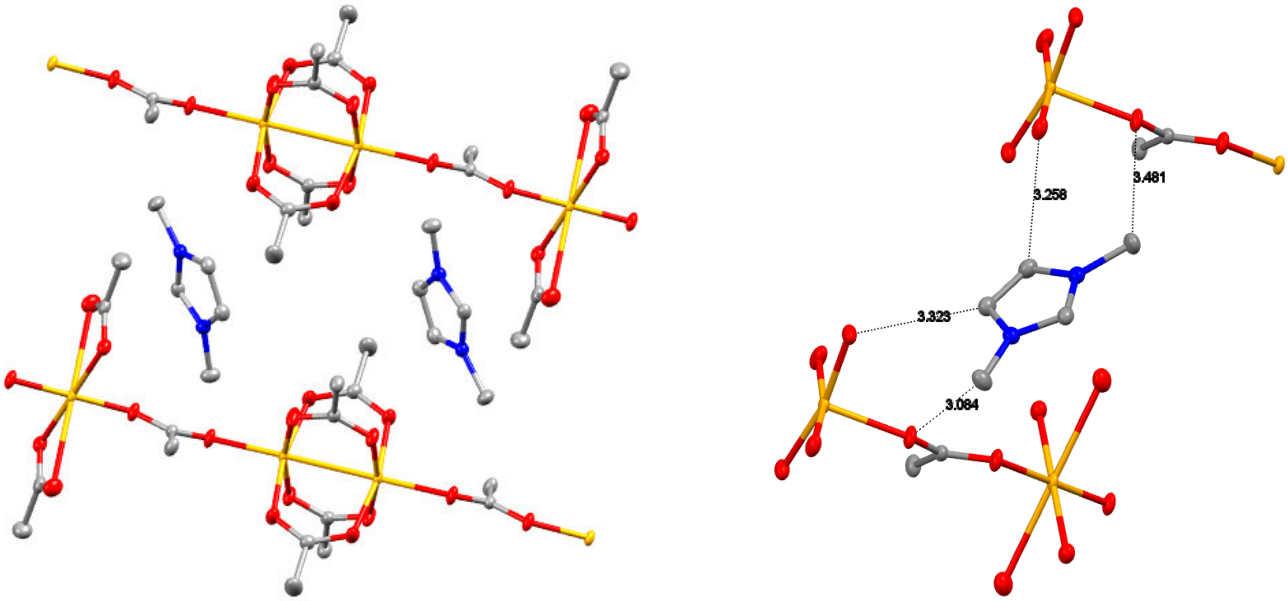

Figure S34. ORTEP representation of the packing of (**4H**)$_2$[$Cu_3(OAc)_8$] (left) and selected atom distances (right). All ellipsoids at 50% probability level; copper atoms in orange; hydrogen atoms and solvent molecules omitted for clarity.

7. Crystallographic details

As a general method, a crystal was mounted in air at ambient conditions. All measurements were made on a *Oxford Diffraction SuperNova* area-detector diffractometer[2] using mirror optics monochromated Mo *K*α radiation (λ = 0.71073 Å) and Al filtered.[3] The unit cell constants and an orientation matrix for data collection were obtained from a least-squares refinement of the setting angles of reflections in the range described for each compound. Frames were collected using ω scans, with a rotation angle of 1.0° per frame, a crystal-detector distance of 65.0 mm, at T = 123(2) K.
Data reduction was performed using the *CrysAlisPro*[2] program. The intensities were corrected for Lorentz and polarization effects, and an absorption correction based on the multi-scan method using SCALE3 ABSPACK in *CrysAlisPro*[2] was applied. Data collection and refinement parameters are given below in tables S4–S7.
The structure was solved by direct methods using *SHELXT*[4], which revealed the positions of all non-hydrogen atoms of the title compound. The non-hydrogen atoms were refined anisotropically. All H-atoms but the two hydroxy ones were placed in geometrically calculated positions and refined using a riding model where each H-atom was assigned a fixed isotropic displacement parameter with a value equal to 1.2Ueq of its parent atom (1.5Ueq for methyl and hydroxyl groups). Refinement of the structure was carried out on F^2 using full-matrix least-squares procedures, which minimized the function $\Sigma w(F_o^2 - F_c^2)^2$. The weighting scheme was based on counting statistics and included a factor to downweight the intense reflections. All calculations were performed using the *SHELXL-2014/7*[4] program in OLEX2.[5] Crystallographic data for all structures have been deposited with the Cambridge Crystallographic Data Centre (CCDC) as supplementary publication numbers 1895828 ([(**2**)$_2$Cu][Cu$_2$(OAc)$_5$(HOAc)]), 1895829 ((**3H**)[Cu$_2$(OAc)$_5$]), 1895830 ((**4H**)$_2$[Cu$_3$(OAc)$_8$]) and 1895831 (**1Br**.CuBr$_2$: **1H.**CuBr$_2$).

Table S4. Crystal data and structure refinement of $[(\mathbf{2})_2Cu][Cu_2(OAc)_5(HOAc)]$.

CCDC No.	1895828
Empirical formula	$C_{56}H_{71}Cl_4Cu_3N_4O_{12}$
Formula weight	1324.58
Temperature/K	123.01(10)
Crystal system	triclinic
Space group	P-1
a/Å	11.7575(2)
b/Å	13.0658(3)
c/Å	21.8616(5)
α/°	99.3392(19)
β/°	100.6079(18)
γ/°	99.4860(16)
Volume/Å^3	3190.96(12)
Z	2
ρ_{calc}g/cm^3	1.379
μ/mm^{-1}	1.216
F(000)	1372.0
Crystal size/mm^3	0.503 × 0.247 × 0.192
Radiation	MoKα (λ = 0.71073)
2Θ range for data collection/°	3.224 to 56.492
Index ranges	$-15 \leq h \leq 15$, $-17 \leq k \leq 17$, $-29 \leq l \leq 28$
Reflections collected	25217
Independent reflections	25217 [R_{int} = ?, R_{sigma} = 0.0610]
Data/restraints/parameters	25217/2/737
Goodness-of-fit on F^2	0.975
Final R indexes [I>=2σ (I)]	R_1 = 0.0463, wR_2 = 0.1140
Final R indexes [all data]	R_1 = 0.0666, wR_2 = 0.1181
Largest diff. peak/hole / e Å^{-3}	1.04/-0.91

Table S5. Crystal data and structure refinement of (**3H**)[$Cu_2(OAc)_5$].

CCDC No.	1895829
Empirical formula	$C_{21}H_{36}Cl_4Cu_2N_2O_{10}$
Formula weight	745.40
Temperature/K	173.00(10)
Crystal system	monoclinic
Space group	$P2_1/c$
a/Å	16.6213(9)
b/Å	17.8406(9)
c/Å	11.3924(5)
α/°	90
β/°	96.223(5)
γ/°	90
Volume/Å^3	3358.3(3)
Z	4
ρ_{calc}g/cm^3	1.474
μ/mm^{-1}	1.632
F(000)	1528.0
Crystal size/mm^3	0.3 × 0.1 × 0.1
Radiation	MoKα (λ = 0.71073)
2Θ range for data collection/°	3.36 to 56.264
Index ranges	-21 ≤ h ≤ 21, -23 ≤ k ≤ 18, -14 ≤ l ≤ 14
Reflections collected	28076
Independent reflections	7488 [R_{int} = 0.0636, R_{sigma} = 0.1200]
Data/restraints/parameters	7488/0/361
Goodness-of-fit on F^2	1.025
Final R indexes [I>=2σ (I)]	R_1 = 0.0827, wR_2 = 0.1881
Final R indexes [all data]	R_1 = 0.1710, wR_2 = 0.2278
Largest diff. peak/hole / e Å^{-3}	0.76/-0.77

Table S6. Crystal data and structure refinement of (**4H**)$_2$[$Cu_3(OAc)_8$].

CCDC No.	1895830	
Empirical formula	C26 H42 Cu3 N4 O16	
Formula weight	857.25	
Temperature	123(2) K	
Wavelength	0.71073 Å	
Crystal system	Triclinic	
Space group	P -1	
Unit cell dimensions	a = 8.5900(3) Å	α= 94.507(3)°.
	b = 9.0259(3) Å	β= 94.617(3)°.
	c = 12.4047(4) Å	γ = 112.873(3)°.
Volume	876.92(5) $Å^3$	
Z	1	
Density (calculated)	1.623 Mg/m^3	
Absorption coefficient	1.877 mm^{-1}	
F(000)	441	
Crystal size	0.298 x 0.234 x 0.059 mm^3	
Theta range for data collection	1.659 to 28.102°.	
Index ranges	-11<=h<=10, -11<=k<=11, -16<=l<=15	
Reflections collected	17915	
Independent reflections	3954 [R(int) = 0.032]	
Completeness to theta = 25.242°	100 %	
Absorption correction	Semi-empirical from equivalents	
Max. and min. transmission	0.8117 and 0.80739	
Refinement method	Full-matrix least-squares on F^2	
Data / restraints / parameters	3954 / 0 / 229	
Goodness-of-fit on F^2	1.043	
Final R indices [I>2sigma(I)]	R1 = 0.0261, wR2 = 0.0637	
R indices (all data)	R1 = 0.0313, wR2 = 0.0666	
Largest diff. peak and hole	0.377 and -0.478 e.$Å^{-3}$	

Table S7. Crystal data and structure refinement of **1H.**$CuBr_2$:**1Br.**$CuBr_2$ 13:87.

CCDC No.	1895831
Empirical formula	$C_{27}H_{36.13}Br_{2.87}CuN_2$
Formula weight	681.59
Temperature/K	173.00(10)
Crystal system	orthorhombic
Space group	$Pna2_1$
a/Å	19.54417(18)
b/Å	12.17073(15)
c/Å	12.47405(14)
α/°	90
β/°	90
γ/°	90
Volume/Å^3	2967.16(6)
Z	4
ρ_{calc}g/cm^3	1.526
μ/mm^{-1}	4.618
F(000)	1366.0
Crystal size/mm^3	0.348 × 0.342 × 0.216
Radiation	MoKα (λ = 0.71073)
2Θ range for data collection/°	3.942 to 56.198
Index ranges	-25 ≤ h ≤ 24, -15 ≤ k ≤ 15, -16 ≤ l ≤ 16
Reflections collected	24694
Independent reflections	6568 [R_{int} = 0.0346, R_{sigma} = 0.0334]
Data/restraints/parameters	6568/1/335
Goodness-of-fit on F^2	1.035
Final R indexes [I>=2σ (I)]	R_1 = 0.0299, wR_2 = 0.0562
Final R indexes [all data]	R_1 = 0.0402, wR_2 = 0.0598
Largest diff. peak/hole / e Å^{-3}	0.28/-0.21
Flack parameter	0.025(9)

8. References

(1) Yun, J.; Kim, D.; Yun, H. A New Alternative to Stryker's Reagent in Hydrosilylation: Synthesis, Structure, and Reactivity of a Well-Defined Carbene-Copper(II) Acetate Complex. *Chem. Commun.* **2005**, No. 41, 5181–5183.

(2) Oxford Diffraction (2010). CrysAlisPro (Version 1.171.38.41). Oxford Difraction Ltd., Yarnton, Oxfordshire, UK.

(3) Macchi, P.; Bürgi, H.-B.; Chimpri, A. S.; Hauser, J.; Gál, Z. Low-Energy Contamination of Mo Microsource X-Ray Radiation: Analysis and Solution of the Problem. *J. Appl. Crystallogr.* **2011**, *44*, 763–771.

(4) Sheldrick, G. M. *SHELXT* - Integrated Space-Group and Crystal-Structure Determination. *Acta Crystallogr. Sect. A* **2015**, *71*, 3–8.

(5) Dolomanov, O. V; Bourhis, L. J.; Gildea, R. J.; Howard, J. A. K.; Puschmann, H. *OLEX2*: A Complete Structure Solution, Refinement and Analysis Program. *J. Appl. Crystallogr.* **2009**, *42*, 339–341.